Deep–Sea Research II 224 (2025) 105555

Contents lists available at ScienceDirect

Deep-Sea Research Part II

journal homepage: www.elsevier.com/locate/dsr2

Indonesian Throughflow into the Leeuwin Current and subtropical Indian Ocean

Asmi M. Napitu *, Arnold L. Gordon, Shannon M. Bohman

Lamont-Doherty Earth Observatory of Columbia University, Palisades, NY, 10964, USA

ARTICLE INFO

Handling Editor: Prof. J Aristegui

ABSTRACT

Indonesian throughflow (ITF) spreads along two major pathways within the Indian Ocean: the westward route within the South Equatorial Current (SEC) and the southward route within the Leeuwin Current (LC) along western Australia. The LC pathway is favored over the SEC pathway when northward winds off the west coast of Australia are weak, such as during Ningaloo Niño in 2010–2014. In this study, we track the ITF spreading into the relatively saline southern Indian Ocean subtropics using the Argo data-derived Relative Fresh Water Content (RFWC) as a marker of ITF water. We contrast the spreading pattern during a strong LC period in 2010–2014 to that during a weak period in 2015–2019. The highest RFWC occurs in the upper 300 m, above the 25.5 kg/m^3 density surface, and migrates westward from the LC as anticyclonic eddies at approximately 4 cm/s. Interannual variability in the RFWC is evident with advective lag times from the LC. The eddies mix their low-salinity ITF water into the salty subtropical water laterally along the density surfaces with an estimated diffusivity rate of 2.4 $\times$ 10^2 m^2/s, affecting the overall freshwater budget of the subtropical gyre. Eddy shedding from the LC system represents an alternative pathway for ITF spreading into the Indian Ocean.

1. Introduction

The major ocean basins exchange water masses within various choke points, which tend to diminish their temperature and salinity differences and shape the global ocean and climate systems (Gordon, 1986, 2001; Schmitz, 1995; Talley, 2013). Interocean links include the Pacific – Indian Ocean exchange within the complex seas and straits of the Maritime Continent, referred to as the Indonesian Throughflow (ITF; Gordon, 2001); Indian – Atlantic exchange around the southern rim of Africa, the Agulhas leakage (Beal et al., 2011); Pacific – Atlantic exchange within the Drake Passage, the Antarctic Circumpolar Current (Döös, 1995); and the smaller but not insignificant in terms of freshwater budgets: Pacific – Atlantic exchange within the Bering Strait (Roach et al., 1995) and the secondary path for Pacific to Indian Ocean exchange along the southern boundary of Australia (Speich et al., 2002).

Besides the water mass composition and property profiles with depth and transport within the interocean passages, there are larger-scale factors that place the interocean exchange in the global ocean perspective. More specifically, the upstream feed into the choke gaps and the downstream spreading patterns from the interocean gaps, what is often referred to as the global ocean conveyor, a conceptual view of the interocean exchange (Broecker, 1987, 1991).

The Agulhas leakage is drawn from the western boundary current of the southern Indian Ocean, the Agulhas Current (Durgadoo et al., 2017). It spreads within the Atlantic Ocean along multiple paths. Some remain in the southern hemisphere within a subtropical super gyre, linking the subtropical gyres of the South Atlantic and Indian Oceans (Speich et al., 2007), and some of the Agulhas water is injected into the North Atlantic, within the upper limb of the Atlantic Meridional Overturning Circulation (AMOC) (Biastoch et al., 2008).

The ITF is drawn from the North and South Pacific Oceans (Hu et al., 2020) via the North/South Equatorial Current (NEC/SEC) and the New Guinea Coastal Current, the Mindanao Current of the North Pacific. The contributions change with depth (e.g., South Pacific water is more common in the lower thermocline) and with the ENSO phase; for instance, the ITF tends to strengthen during La Niña (Gruenburg and Gordon, 2018; Gordon et al., 2019).

The ITF water enters the Indian Ocean (Sprintall et al., 2024), mainly spreading westward within the South Equatorial Current (SEC; Gordon et al., 1997; Song et al., 2004) and along a secondary route southward

This article is part of a special issue entitled: IIOE2 V9 published in Deep-Sea Research Part II.

* Corresponding author.
E-mail address: asminapitu@caa.columbia.edu (A.M. Napitu).

https://doi.org/10.1016/j.dsr2.2025.105555
Received 3 January 2025; Received in revised form 30 September 2025; Accepted 16 October 2025
Available online 17 October 2025

along the west coast of Australia within the Leeuwin Current (LC; Church et al., 1989; Godfrey and Ridgway, 1985, Fig. 1a). The ITF water within the SEC, upon reaching the western Indian Ocean, bifurcates, with some spreading northward into the Arabian Sea (Song et al., 2004) and some southward into the Agulhas Current. The LC flows southward in the surface and upper thermocline. Below ~200 m, the Leeuwin Undercurrent flows northward. The low-salinity ITF water, primarily above the density surface of 25.5 kg/m^3, that enters the LC feeds into the subtropical gyre of the southern Indian Ocean (Furue et al., 2017), inducing a fresher subtropical gyre, which eventually enters the Agulhas Current.

Once the ITF enters the Indian Ocean off the Australian Northwest coast, it spreads across the Indian Ocean within the SEC and with a smaller amount flowing southward along the west coast of Australia within the LC. The ratio between the two pathways, which varies seasonally and interannually, depends on the ocean dynamics of the eastern tropical Indian Ocean, as well as the larger-scale wind field. Gruenburg et al. (2023) argued that the LC path is favored during Ningaloo Niño events when the winds off the Australian Northwest coast are cyclonic (clockwise) and the northward winds off the west coast of Australia are weak, as occurred in 2000 and 2011.

Our study traces the spreading of the low-salinity ITF water into the subtropical Indian Ocean. Specifically, we aim to detect the ITF imprints in the southern Indian Ocean subtropical gyre, originating from the LC current system along the western Australian continental shelf. Sections 2 and 3 will describe the data and methods to trace the ITF water and discuss its manifestations in the LC system, including contrasting the ITF water properties during strong and weak LC conditions. We will discuss evidence of the ITF water in the subtropical gyre and respective underpinning physical processes in Section 4. Summary and Discussion in Section 5 concludes the paper.

2. Data and methods

To trace the ITF properties contemporaneously with changes in the strength of the LC and mesoscale eddies, we analyzed quality-controlled Argo Temperature [T] and Salinity [S] profiles in the southeastern Indian Ocean within 18–35°S and 90–115°E throughout 2004–2020. The Argo T and S observations were obtained and archived by the International Argo Program, part of the Global Ocean Observing System (https://www.ocean-ops.org/board), from which we computed the conservative T, absolute S, sigma-density [σ_0], and Relative Fresh Water Content (RFWC) in the upper 500 m. The calculation of the RFWC in a given area involves a four-step process. First, σ_0 profiles in the upper 500 m of the area were computed from the Argo T and S data. Second, the Argo S data were grouped into σ_0 surfaces with increments of 0.1 kg/m^3. Third, within each σ_0 surface or layer, the maximum and minimum values of the S data (S_{max} and S_{min}, respectively) were identified. Fourth, the S data were normalized to a range of 0–1. This normalization was achieved by subtracting S_{min} from each S value and then dividing the result by the data range (S_{max} - S_{min}). These normalized S values represent the RFWC, where a value of 0 indicates salty subtropical Indian Ocean water, and a value of 1 signifies pure ITF water. The available Argo floats during the observational period are shown in Fig. 2a.

In addition to the Argo observations, we examined daily satellite sea surface height (SSH) anomalies data distributed by the Copernicus Marine Service, provided on a 0.25° longitude-latitude grid (Taburet et al., 2019). The SSH data were utilized to detect eddy activity off the Australian west coast, mainly to track westward eddy movement into the subtropical water.

We computed probability density function (PDF) estimates of T, S, and σ_0. The PDF estimate is the number of occurrences of a value in the data range normalized by the total number of data points and the bin width. We applied a Gaussian Kernel Density Estimation method to estimate the PDF (Terrell and Scott, 1992).

3. Injection of low-salinity ITF water into the LC

The poleward flow of the LC is attributable to a balance between the poleward pressure gradient along the western Australian continental shelf and the equatorward wind and bottom stresses (Smith et al., 1991; Waite et al., 2007). The buoyant (low-salinity and warm) waters of the ITF raise the sea level at the Northwest Australian coast, inducing the poleward pressure gradient. Moreover, coastal trapped waves spread the elevated sea level poleward, establishing a zonal pressure gradient along the west coast of Australia, which drives poleward geostrophic currents, which also sustain the LC (Kundu and McCreary Jr, 1986; Furue et al., 2017). In addition to the alongshore pressure gradient and stresses, Feng et al. (2005) indicated that mesoscale eddies contribute to the momentum balance of the LC system.

In addition to the alongshore mechanisms, cross-shelf exchanges also modify the LC. The shallow Eastern Gyral Current [EGC; Fig. 1a] also feeds into the LC. Mesoscale eddies generated off the western Australian coast transfer LC properties westward into the subtropical gyre of the southern Indian Ocean (Fang and Morrow, 2003; Domingues et al., 2006). Eddy heat fluxes into the ocean interior account for about 70 % of the observed 5 °C cooling of the LC along the west Australian coast (Ridgway and Condie, 2004; Domingues et al., 2006).

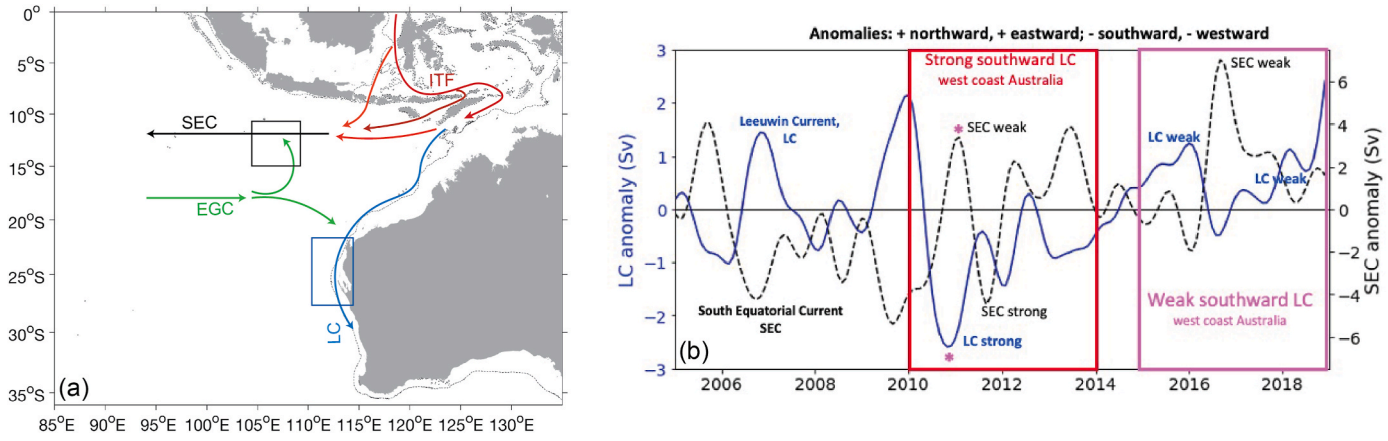

Fig. 1. (a) Schematic of the major ocean currents in the southeast Indian Ocean. The red, black, blue, and green arrows indicate the Indonesian Throughflow (ITF), South Equatorial Current (SEC), Leeuwin Current (LC), and Eastern Gyral Current (EGC). (b) The LC (blue line) and SEC (dashed black line) transport anomalies above the 25.5 kg/m^3 density surface during the Argo observational period. The maximum in southward (negative anomaly values are northward) LC transport anomaly in 2011 matches a minimum in westward (positive anomaly values are eastward) SEC transport anomaly. The LC and SEC transport time series, inferred from general circulation model velocities within the blue and black rectangles, are adapted from Fig. 8 of Gruenburg et al. (2023).

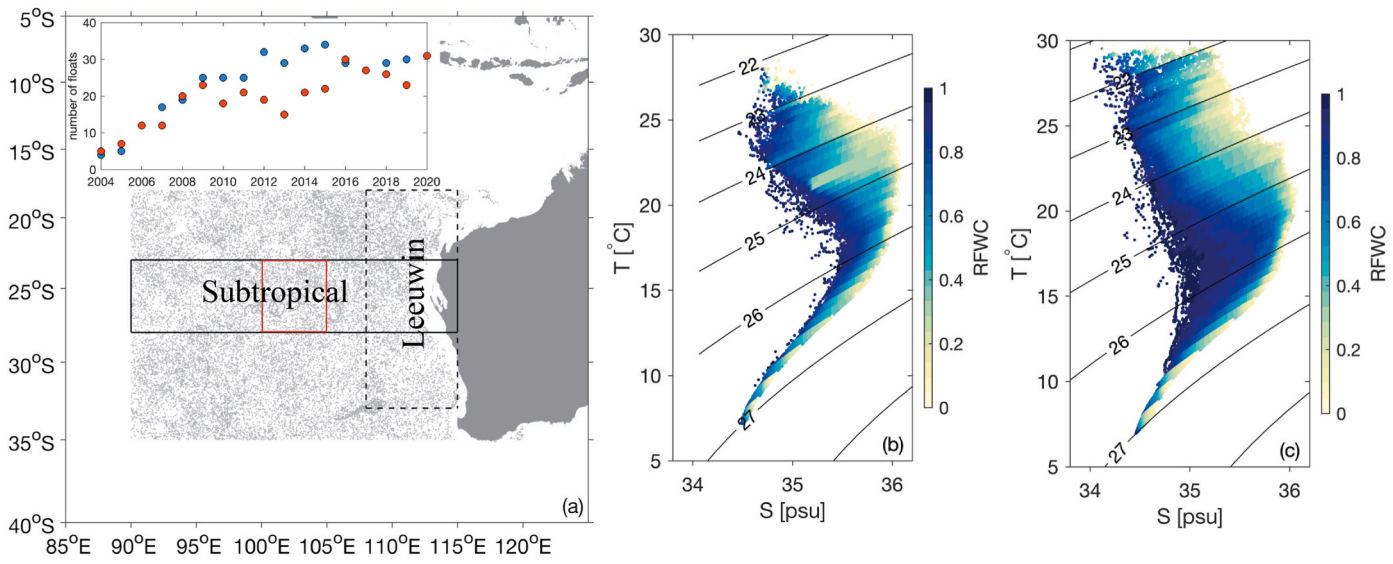

Fig. 2. (a) Gray dots indicate the nominal location of Argo floats operational during 2004–2020 in the study region. (b) T-S diagram color coded relative freshwater content [RFWC] computed at a 0.1 kg/m^3 increment based on the Argo data bounded by the solid black (subtropical) rectangle in (a). (c) Like in (b) but for the Argo data within the dashed black (Leeuwin) rectangle in (a). The red rectangle in (a) marks the central area of the subtropical rectangle. The inset in (a) shows the annual number of Argo floats in the subtropical rectangle (blue) and the Leeuwin rectangle (red).

To estimate the injection of the ITF water into the LC and onto the subtropical gyre, we examined the Argo data off the western Australian coast, specifically within the area marked by the dashed and solid rectangles shown in Fig. 2a. Fig. 2b shows the T-S diagram, color-coded for RFWC, for a subset of the subtropical area where the LC influence is most pronounced within the latitude band of 23–28°S (Kersalé et al., 2022; Gruenburg et al., 2023). The T-S diagram off the west coast of Australia, Fig. 2c, exemplifies the RFWC between 18 and 33°S and 108–115°E. The T-S diagrams showcase the relatively fresh ITF marker as dark blue, whereas the salty subtropical water is indicated by light yellow. However, we emphasize that not all T-S data with high RFWC values represent the low-salinity and warm ITF water, particularly below 25.5 σ_0 marking the lower thermocline. We will focus on the RFWC from the sea surface to the 25.5 σ_0 isopycnal where the ITF imprint is strongest.

The LC exhibits variability across a broad range of timescales, predominantly annual and interannual variations. Feng et al. (2003) reported that the LC transport is largest during June and July when the northward-directed wind is weakest. The same study also found that the transport was strongest during La Niña years, concomitant with increased sea level along the western Australian coast induced by greater ITF transport, which enhances seaward pressure gradient and, thereby, southward geostrophic current.

Feng et al. (2013, 2015) suggested a surge in the LC transport, associated with an increase in the ITF transport, responding to strong La Niña years in 2010–2011 which also explains unprecedented SST warming by up to 5 °C off the west coast of Australia, causing widespread impacts on marine ecosystem. They coined the anomalous condition as Ningaloo Niño. More recently, Gruenburg et al. (2023) indicated that the stronger LC transport in 2011 coincided with the weakening of the SEC. They argued that a cyclonic atmospheric circulation off the northwest Australian coast during a very strong Ningaloo Niño from 2010 to 2013 contributed to the reversal of the SEC and the strengthening of the LC. Conversely, a strong SEC-weak LC relationship was observed during 2015–2018, as the cyclonic winds diminished.

Comparing the Argo data for the strong LC period from 2010 to 2014 with that for the weak LC period from 2015 to 2019 reveals distinct features in the hydrography attributable to the two LC periods. Analysis of the Argo T and S data within the subtropical rectangle (solid line) in Fig. 2a indicates greater occurrences of fresher and warmer water, characteristic of the ITF, during strong LC transport (Fig. 3a), with predominant T = 21 °C and S = 35.2 psμ peaks (Fig. 3c and d), induced by increased ITF inflow. The S = 35.7 psμ peak (Fig. 3d) is indicative of the salty subtropical water. The salinity peak is observed within the subtropical rectangle regardless of the LC strength.

The value of the ITF marker at the salinity peak value is not as low as observed in the SEC, with S = 34.8 psμ (Gordon et al., 1997), a likely consequence of the presence of salty subtropical effect within the LC. Upper ocean freshwater loss due to decadal variability in the Southeast Indian Ocean after 2011, as reported by Li et al. (2023), might also explain the saltier ITF water observed in the LC system by Argo floats. Fig. 3e demonstrates more T and S data occurrence within the water column above the density surface of 25.5 kg/m^3 during the strong LC transport. In contrast, those deeper than the density surface of 26 kg/m^3 are predominant during the weak LC transport periods.

The Argo data within the rectangle along the west coast of Australia (Fig. 2a) reveal warm temperature (T > 22 °C) and low salinity (S < 34.6 psμ) water, different from the T/S during the strong LC period from the weak period (Fig. 4a–c). However, the strong LC period along the coast is uniquely characterized by a T range of 16-18 °C, an S range of 35.6–35.7 psμ, and a σ_0 range of 25.9–26.1 kg/m^3. It is unlikely that those values represent the ITF water. The T/S is close to those of the Indian Ocean subtropical mode water (IOSTMW) in the LC system (Adiwira and Suga, 2023). The formation of the IOSTMW occurs along the northern flank of the Agulhas Return Current in the southwest Indian Ocean (Toole and Warren, 1993). The South Indian Counter Current advects it from the formation region eastward to the west coast of Australia (Menezes et al., 2016). In addition to the IOSTMW, the high salinity peak (Fig. 4c) could indicate increased exchange, potentially facilitated by eddies, between the LC water and the surrounding open-ocean subtropical water (Feng et al., 2005).

From the surface layer to the 25.5 σ_0, the RFWC in the subtropical rectangle in Fig. 2a for the contrasting strong and weak LC periods reveals increased freshening effect during strong LC (Fig. 5). The relative fresh ITF water with S < 34.8 psμ was observed in the LC system more frequently during the strong LC period than during the weak LC period (Fig. 5a and b). The distributions of the RFWC are visually different, with a narrow peak centered at RFWC = 0.65 marking that for the strong LC. Furthermore, a Kolmogorov-Smirnov test confirms that the distributions of the RFWC for the strong and weak LC periods are statistically

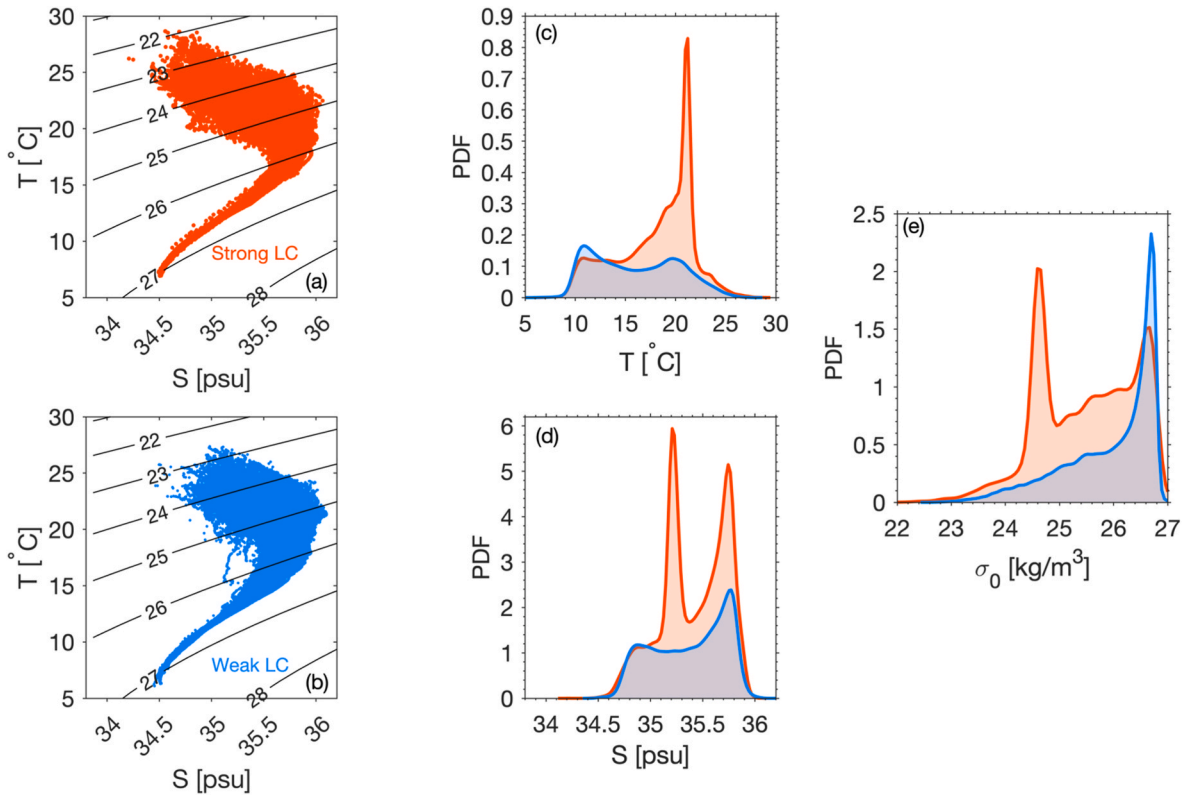

Fig. 3. Contrasting T, S, and σ_0 features for the strong and weak LC periods observed in the subtropical rectangle shown in Fig. 2a. The T-S diagram for the strong LC period (a) and the weak LC period (b). The Probability Density Function [PDF] estimate of T (c), S (d), and σ_0 (d), color coded for the strong LC period (red) and the weak LC period (blue).

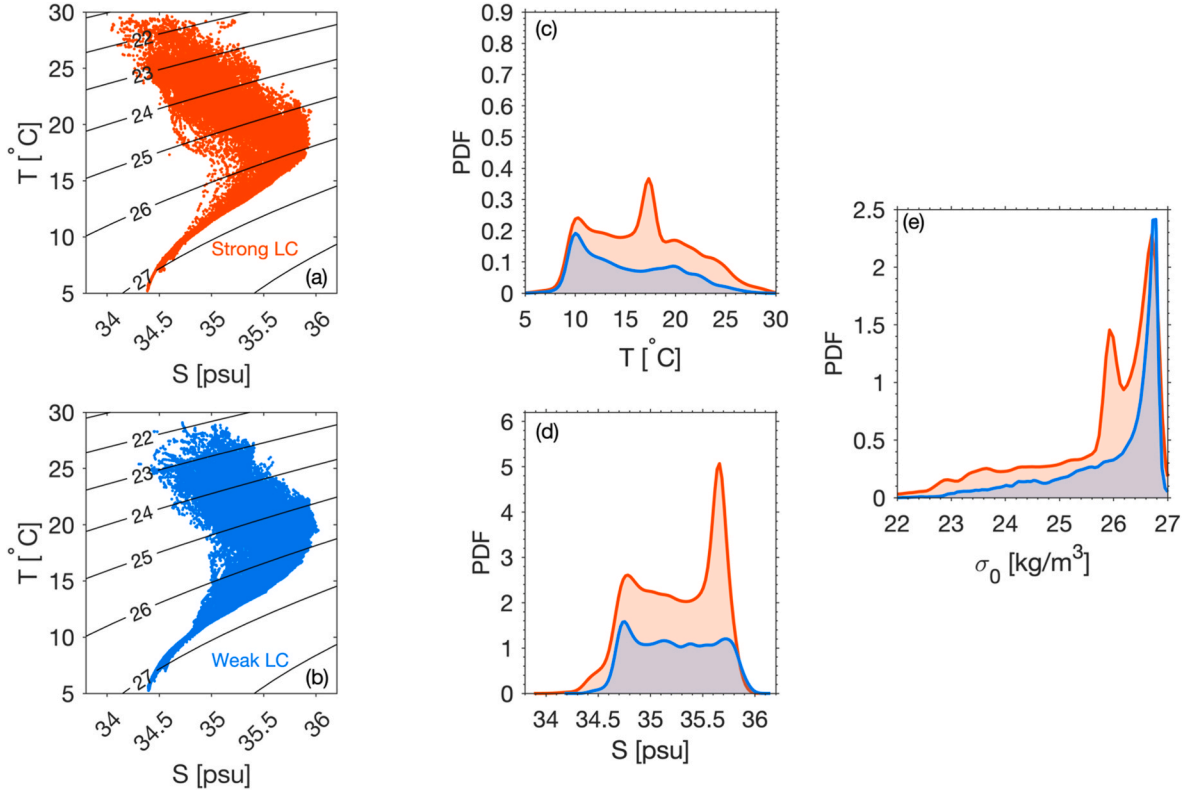

Fig. 4. As in Fig. 3 but inferred from the Argo data observed within the Leeuwin rectangle (dashed) shown in Fig. 2a.

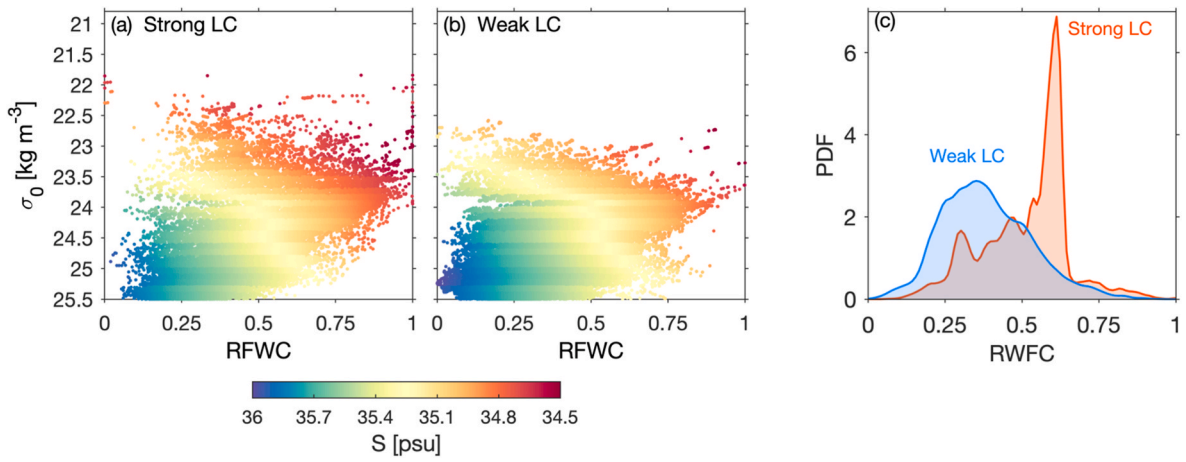

Fig. 5. (a and b) Scatter plots of RFWC versus σ_0 inferred from the Argo data within the area bounded by the subtropical rectangle in Fig. 2a for the strong LC period (a) and the weak LC period (b). (c) The Probability Density Function [PDF] estimate of the RFWC for the strong (orange) and weak (blue) LC periods.

different (Fig. 5c).

4. RFWC westward spread and mixing into the south Indian Ocean subtropical gyre

4.1. An overview of RFWC westward spreading

Previous studies reported that a more energetic LC corresponds with an increase in eddy shedding from the coastal boundary flow, permitting a cross-shore transport of heat and freshwater from the continental shelf to the ocean interior (Fang and Morrow, 2003; Domingues et al., 2006). Traces of low salinity ITF water (RFWC >0.7) are observable off the continental shelf during the strong LC period (Fig. 6a–d), particularly from the surface down to the density surface of 25.5 kg/m^3. On the contrary, salty subtropical water, marked by low RFWC values (RFWC<0.3), dominates the observations in the ocean interior during weak LC (Fig. 6e–h).

The spreading of the ITF water from the LC, confined within the continental margin of the Australian west coast, to the subtropical water is likely commensurate with the increased activity of eddy shedding from the boundary current. Increased LC transport would facilitate the detachment of more eddies from the continental shelf, thereby increasing eddy fluxes that advect and mix the ITF water into the subtropical interior. Another ocean dynamic that could transfer the ITF water into the open ocean is wind-forced Rossby waves, which are reportedly more energetic during the strengthened LC period (Furue et al., 2017; Zheng et al., 2018).

4.2. RFWC westward spreading rate

To further test the hypothesis that ITF water spreads into the interior, we tracked changes in the RFWC mid-thermocline (averaged between $\sigma_0 = 24.5$ kg/m^3 and $\sigma_0 = 25$ kg/m^3) within the latitude of 18°S and 35°S at four different longitude bands, 111°-114°E, 105°-108°E, 99°-102°E,

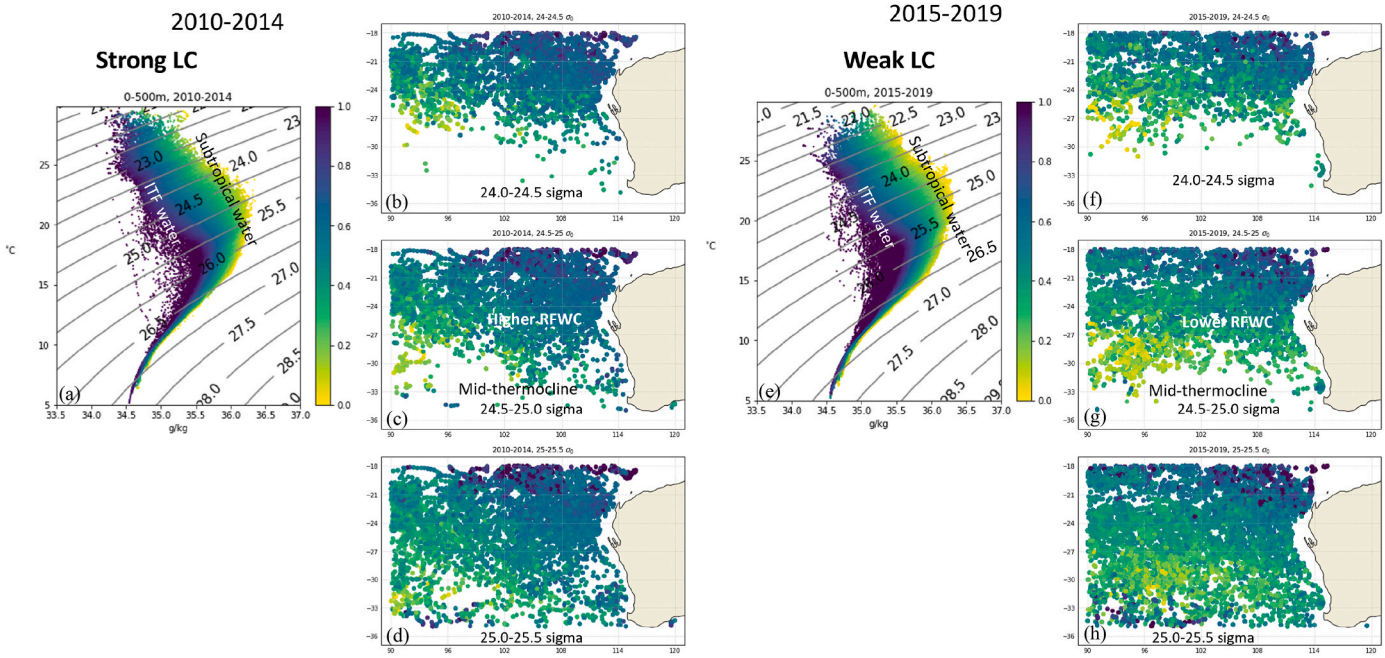

Fig. 6. The T-S diagram, color-coded with the respective RFWC, observed by Argo floats off the west Australian coast between 90°E and 115°E and between 18°S and 36°S during the strong LC in 2010–2014 (a) and during the weak LC in 2015–2019 (e). The RFWC inferred from the Argo floats during the strong LC period at three density slabs, 24.0–24.5 kg/m^3 (b), 24.5–25.0 kg/m^3 (c), and 25.0–25.5 kg/m^3 (d). (f, g, and h) As in (b), (c), and (d), but for the weak LC period.

93°-96°E. The choice of the longitude bands allows for tracking ITF water as it spreads westward. The time-series of the monthly RFWC values averaged in the longitude band 111°-114°E show enhanced values during 2010–2014 (Fig. 7a), relative to those in the rest of the observational period, simultaneous with the strengthened LC period.

The smoothed RFWC time series (the gray curve in Fig. 7a) indicates that the highest RFWC values exceeding 0.7 were observed in 2011–2012. Moreover, the best fit to the smoothed RFWC timeseries (red dashed line in Fig. 7a) for the 2010–2014 period demonstrates a peak in July 2012, implying the water column in the longitude band was freshest around the time concurrent with the period when the LC attained its maximum southward transport in 2012 (Gruenburg et al., 2023).

Further to the west, traces of the low-salinity ITF water were also observed but later in the year. For example, the RFWC values averaged in the longitude band 105° −108°E observed in 2010–2014 tended to be higher than those in other years (Fig. 7b). The best fit to the smoothed RFWC values in the 2010–2014 period shows a peak in November 2012. Thus, there is a four-month delay between the RFWC peak in the longitude band 111°-114°E and that in the longitude band 105° −108°E, which implies a westward drift of the ITF water with a speed of ~4 cm/s. In the two westernmost longitude bands, the period of increased low salinity ITF water in 2010–2014 is essentially absent (Fig. 7c and d).

Past studies reported that the phase speeds of the observed eddies in the region vary between 2 and 5 cm/s (Fang and Morrow, 2003; Waite et al., 2007). Chelton et al. (2007) showed that the latitude band between 20°S and 35°S is an energetic Rossby wave latitude band, with an

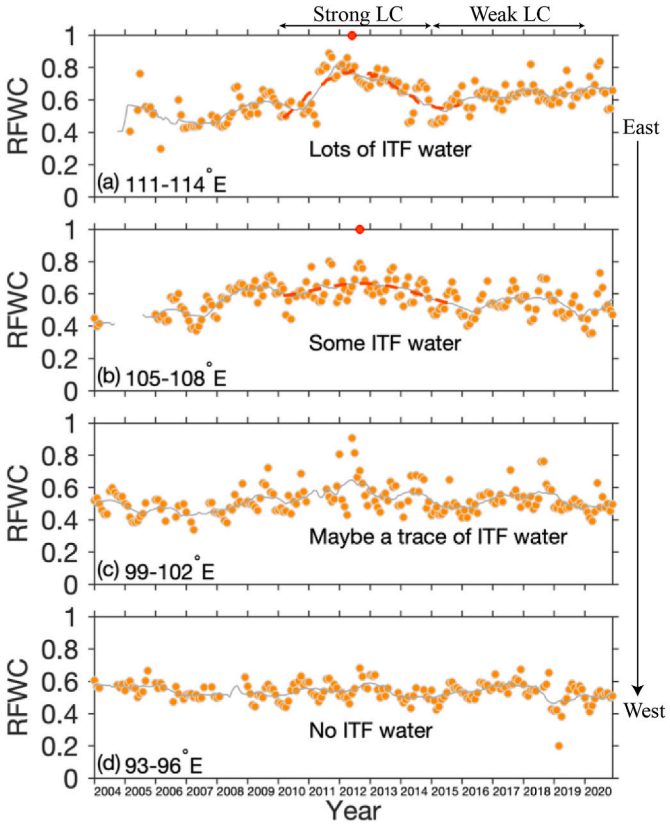

Fig. 7. Time series of the RFWC laterally averaged in the region within a latitude band between 18°S and 35°S and a longitude band between 111°-114°E (a), 105°-108°E (b), 99°-102°E (c), and 93°-96°E (d) and vertically averaged between the density surface of 24.5 kg/m^3 and the density surface of 25 kg/m^3 during 2004–2020. The gray line represents the smoothed RFWC time series, whereas the red dashed line is the fitted curve to the smoothed time series for a specific period between 2010 and 2014. The red dot indicates the peak of the fitted curve.

average phase speed of Rossby waves emanating from the eastern boundary in the subtropical Indian Ocean of 4 cm/s. Since the observed westward drift of the ITF water inferred from the RFWC time series shown in Fig. 7a and b is within the measured range of the eddy phase speeds, the westward drift of the RFWC is likely a product of transient eddies.

4.3. SSH relation to RFWC

As discussed above, analysis of the Argo-derived RFWC values within the eastern subtropical regime of the Indian Ocean reveals an increased concentration of low-salinity ITF water from 2010 to 2014, with a peak between summer and fall 2012, which coincided with a period of strengthened LC transport along the western Australian continental shelf. We now investigate the SSH anomalies off the Australian west coast to explore the cross-shelf and slope transfer of ITF water into the ocean interior. As a first approximation, we examined the lowpass-filtered SSH anomalies, with seasonal and shorter than 30-day variations removed, focused on the latitude band of 23°-27°S. The preferred latitude band is one of the three latitude bands, with the other two bands being between 20° and 21°S and between 28° and 31°S, where eddy shedding from the LC has been observed (Fang and Morrow, 2003).

The SSH anomalies averaged in the latitude band of 23°-27°S demonstrate the recurrence of zonally propagating pulses (Fig. 8a). Bands of SSH anomalies with opposing polarities propagate westward with an average phase speed of about 4 cm/s. The westward-propagating feature emanating from the eastern boundary was particularly more pronounced during 2011–2013, marked by positive anomalies with magnitudes exceeding 10 cm relative to other years. Its maximum signature appeared in 2012 when the subtropical water was recorded as freshest.

The elevated SSH anomalies, associated with anticyclonic eddies, drift westward. Fig. 8b and c shows the evolution of an anticyclonic eddy generated off the western Australian coast, with an amplitude exceeding 10 cm. The eddy grows in size, with its radius increasing from 40 km to 80 km, as it shifts westward at a speed of about 4 cm/s, similar to the average speed inferred from Fig. 8a.

To further assess the role of eddies, particularly the anticyclonic ones, in freshening the subtropical water, we contrasted the RFWC values in an area between 23 and 27°S and between 110 and 115°E shown in Fig. 2a during the strong anticyclonic eddy period in 2011–2014 to those when the eddy activity is weaker in other years. The results indicate that Argo profiles detect more events with low salinity ITF water, high RFWC, during the strong eddy activity period than during the weak period (Fig. 9).

4.4. Mixing of high RFWC ITF water into the regional subtropical gyre of the southern Indian Ocean

As the eddies from the LC migrate westward at a rate of ~4 cm/s (Fig. 8a), the relatively low salinity within the eddy pycnocline gradually attenuates as it mixes into the more saline regional subtropical water. As shown in Fig. 7, the signature RFWC of the ITF water is removed, decreasing from 0.8 to 0.6 from the 111–114°E to 105–108°E longitude, a 6° longitude shift at 25°S, which at 4 cm/s represents a journey of ~4 months. The decreased RFWC amounts to an increase of salinity at the eddy core of 0.15 (Fig. 2). Estimating the radius of the eddy ~50 km and a surrounding transition from high RFWC to regional salinity (Fig. 8b and c) of ~100 km, we estimate the isopycnal mixing coefficient (k_h/ρ) within the transition from the eddy core to the regional subtropical water to be 2.4 × 10^2 m^2/s, which is characteristic of ocean mesoscale.

The leakage of LC water, enriched with low salinity ITF water, into the subtropical regime of the southern Indian Ocean acts to reduce the subtropical salinity. This can be expressed as equivalent precipitation. The precipitation in the eastern subtropical regime, spanning 115°E to

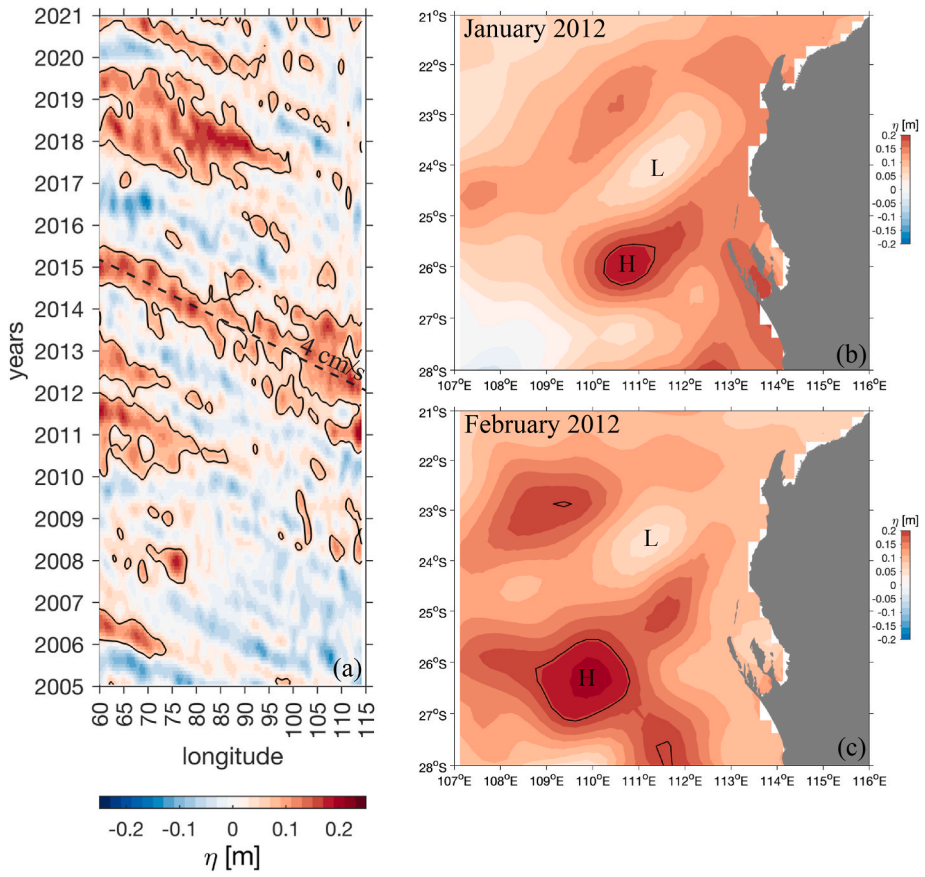

Fig. 8. Hovmoller diagram of the SSH (a) anomalies averaged within the 23–27°S band. (b and c) Snapshots of SSH anomalies in January 2012 (b) and February 2012 (c). The contours in (b and c) mark the SSH anomalies = 0.1 m, whereas the black dashed line in (a) shows the linear fit to the SSH anomaly contours during 2012–2014. The "H" and "L" labels in (b) and (c) mark high and low SSH anomalies.

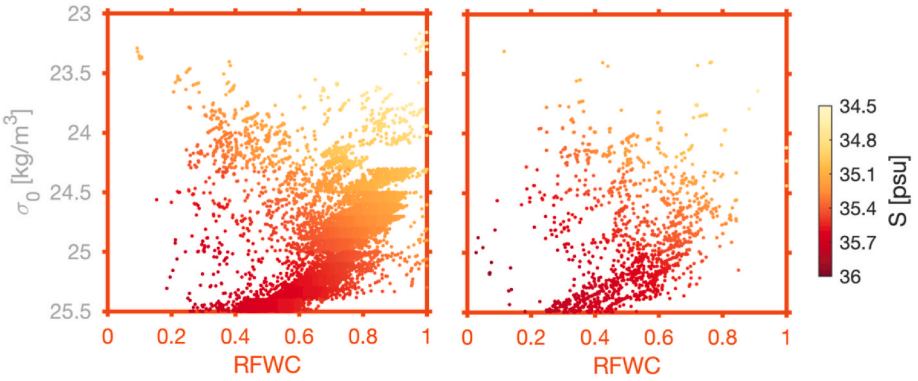

Fig. 9. The RFWC in the central part (red square) of the subtropical rectangle shown in Fig. 2a for the periods of strong anticyclonic eddies (left panel) and weak eddies (right panel).

90°E and 20°S to 35°S, where the ITF water blends into the regional subtropical water, is ~0.2 m/year (Schanze et al., 2010). The salinity difference between the low salinity ITF enriched water and the saline subtropical water is ~1 psμ or ~1 ppt. Thus for 0.001 kg of salt in a kilogram of sea water, there is 0.999 kg of freshwater. Thus for 10 Sv of ITF water within the LC (approximate ITF inflow to the LC enriched for periods of strong input) injected into the subtropical water, the freshwater addition expressed as equivalent precipitation over the eastern subtropical area amounts to 0.075 m/year, or ~37 % of the air to sea precipitation. This drops to near zero when the ITF flows into the SEC.

5. Conclusions and discussion

The relatively low-salinity ITF water injected into the LC displays interannual variability. From 2005 to 2020, we find that the maximum inflow occurred from late 2010 into 2013, with peak injection in 2011. The ITF water turns into the LC rather than advect westward within the SEC when the northward winds off the west coast of Australia are weak, as occurred during the La Nina of 2010–2011. The ITF water spreads westward from the LC at speeds of ~4 cm/s, representative of Rossby Waves, into the relatively saline subtropical regime of the southern Indian Ocean. The high RFWC of the ITF-enhanced LC gradually blends into the subtropical regional water via lateral mixing. This process

effectively reduces the sea-air exchange positive Evaporation minus Precipitation (E-P) of the subtropical regime.

The subtropical regime with its high sea surface salinity (SSS) characteristic of the southern Indian Ocean differs from the SSS-max subtropical water of the other ocean basins. The southern Indian Ocean SSS-max centered near 30°S is in a more poleward position than the subtropical SSS-max of the Pacific and Atlantic Oceans and poleward of the high E–P band near 20°S (Gordon et al., 2015; Vinogradova et al., 2019), a consequence of the low salinity ITF water that advects westward in the SEC near 12°S (Gruenburg et al., 2023). The southward-flowing LC, driven by the higher sea level off the northwest coast of Australia, inhibits the inflow of subpolar water from the south. As shown above, the LC at times is enhanced with lower salinity water by the injection of ITF water along the northwest coast of Australia, which impacts the southern Indian Ocean SSS-max. In addition, unlike the SSS-max regime of the Pacific and Atlantic Oceans, the saline subtropical water reaches eastern boundary, the west coast of Australia, as the low SSS subpolar water does not flow towards the equator in the eastern boundary as is the situation in the other ocean basins (Gordon et al., 2015). Relatively salty water may also enter the LC along the southern coast of Australia, derived from the Tasman Sea (van Sebille et al., 2014).

Bingham et al. (2023) investigated the seasonal and interannual variability of the centroid of the subtropical southern Indian Ocean during 2004–2020. They found that the centroid shifts northward (southward) in winter (summer). On the interannual time scale, the area of the SSS-max was greatest in 2006, reached a minimum in 2013, increased after that year, and reached a secondary peak in 2017 (see Fig. 8 of Bingham et al. (2023)). This is quite consistent with our findings of the increased RFWC into the LC in 2010–2011, with a lag time due to the westward spreading of the LC water. We propose that the decrease in the SSS-max area and salinity reported by Bingham et al. (2023) is a result of the ITF-enhanced, lower salinity water spreading westward from the LC in 2011–2012.

The injection of ITF water into the LC and onto the southern Indian Ocean subtropics represents an alternative pathway of ITF spreading within the Indian Ocean to the westward pathway within the SEC. Whereas the SEC delivers the ITF water into the tropical western Indian Ocean (Song et al., 2004), the LC pathway injects relatively low salinity water into the southern subtropical thermocline, which may be passed onto the western boundary Agulhas Current potentially to add to the Agulhas leakage around the southern rim of Africa, and AMOC (Gordon, 1986). This topic may be explored through Argo and reanalysis data, as well as model simulations, across the Indian Ocean.

CRediT authorship contribution statement

Asmi M. Napitu: Writing – review & editing, Writing – original draft, Visualization, Validation, Methodology, Investigation, Formal analysis, Data curation, Conceptualization. **Arnold L. Gordon:** Writing – review & editing, Validation, Supervision, Methodology, Investigation, Funding acquisition, Formal analysis, Conceptualization. **Shannon M. Bohman:** Visualization, Formal analysis, Data curation.

Declaration of competing interest

The authors declare that they have no known competing financial interests or personal relationships that could have appeared to influence the work reported in this paper.

Acknowledgement

We acknowledge constructive comments from two anonymous reviewers and Dr. Kandaga Pujiana on an earlier version of the manuscript. The research was funded by NSF grant OCE-2242195 "Collaborative Research: A New Pathway of Indonesian Throughflow in the Indian Ocean, and ONR grant N00014-22-1-2586, The Northern Embayments of the Indian Ocean and the Indonesian Throughflow.

References

Adiwira, H., Suga, T., 2023. The interannual variability of the Indian Ocean subtropical mode water based on the argo data. Front. Mar. Sci. 10, 1205292.
Beal, L.M., De Ruijter, W.P., Biastoch, A., Zahn, R., 2011. On the role of the agulhas system in ocean circulation and climate. Nature 472 (7344), 429–436.
Biastoch, A., Böning, C.W., Lutjeharms, J.R.E., 2008. Agulhas leakage dynamics affects decadal variability in Atlantic overturning circulation. Nature 456 (7221), 489–492.
Bingham, F.M., Brodnitz, S.K., Gordon, A.L., 2023. Seasonal and interannual variability of the subtropical South Indian Ocean sea surface salinity maximum. J. Geophys. Res.: Oceans 128 (2), e2022JC018982.
Broecker, W.S., 1987. The biggest chill. Nat. Hist. 97, 74–82.
Broecker, W.S., 1991. The great ocean conveyor. Oceanography (Wash. D. C.) 4 (2), 79–89. https://doi.org/10.5670/oceanog.1991.07.
Chelton, D.B., Schlax, M.G., Samelson, R.M., de Szoeke, R.A., 2007. Global observations of large Oceanic eddies. Geophys. Res. Lett. 34 (15).
Church, J.A., Cresswell, G.R., Godfrey, J.S., 1989. The leeuwin current. In: Neshyba, S.J., Mooers, C.N.K., Smith, R.L., Barber, R.T. (Eds.), Poleward Flows Along Eastern Ocean Boundaries, Coastal Estuarine Stud, 34. AGU, Washington, D.C., pp. 230–254
Döös, K., 1995. Inter-ocean exchange of water masses. J. Geophys. Res. 100 (C7), 13 499–13 514.
Domingues, C.M., Wijffels, S.E., Maltrud, M.E., Church, J.A., Tomczak, M., 2006. Role of eddies in cooling the Leeuwin Current. Geophys. Res. Lett. 33 (5).
Durgadoo, J.V., Rühs, S., Biastoch, A., Böning, C.W.B., 2017. Indian Ocean sources of agulhas leakage. J. Geophys. Res.: Oceans 122, 3481–3499. https://doi.org/10.1002/2016JC012676.
Fang, F., Morrow, R., 2003. Evolution, movement and decay of warm-core Leeuwin Current eddies. Deep Sea Res. Part II Top. Stud. Oceanogr. 50 (12–13), 2245–2261.
Feng, M., Meyers, G., Pearce, A., Wijffels, S., 2003. Annual and interannual variations of the Leeuwin Current at 32 S. J. Geophys. Res.: Oceans 108 (C11).
Feng, M., Wijffels, S., Godfrey, S., Meyers, G., 2005. Do eddies play a role in the momentum balance of the Leeuwin Current? J. Phys. Oceanogr. 35 (6), 964–975.
Feng, M., McPhaden, M.J., Xie, S.P., Hafner, J., 2013. La Niña forces unprecedented Leeuwin Current warming in 2011. Sci. Rep. 3 (1), 1277.
Feng, M., Benthuysen, J., Zhang, N., Slawinski, D., 2015. Freshening anomalies in the Indonesian throughflow and impacts on the Leeuwin Current during 2010–2011. Geophys. Res. Lett. 42 (20), 8555–8562.
Furue, R., Guerreiro, K., Phillips, H.E., McCreary Jr., J.P., Bindoff, N.L., 2017. On the Leeuwin Current system and its linkage to zonal flows in the south Indian Ocean as inferred from a gridded hydrography. J. Phys. Oceanogr. 47 (3), 583–602.
Godfrey, J.S., Ridgway, K.R., 1985. The large-scale environment of the poleward-flowing Leeuwin Current, Western Australia: longshore steric height gradients, wind stresses, and geostrophic flow. J. Phys. Oceanogr. 15, 481–495.
Gordon, A.L., 1986. Interocean exchange of thermocline water. J. Geophys. Res. 91, 5037–5046. https://doi.org/10.1029/JC091iC04p05037.
Gordon, A.L., 2001. Interocean exchange. Chapter 4.7. In: Siedler, G., Church, J., Gould, J. (Eds.), Ocean Circulation and Climate. Academic Press, pp. 303–314.
Gordon, A.L., Giulivi, C.F., Busecke, J., Bingham, F.M., 2015. Differences among subtropical surface salinity patterns. Oceanography (Wash. D. C.) 28 (1), 32–39.
Gordon, A.L., Ma, S., Olson, D.B., Hacker, P., Ffield, A., Talley, L.D., Wilson, D., Baringer, M., 1997. Advection and diffusion of Indonesian throughflow within the Indian Ocean south equatorial Current. Geophys. Res. Lett. 24 (21), 2573–2576.
Gordon, Arnold L., Napitu, Asmi, Huber, Bruce A., Gruenburg, Laura K., Pujiana, Kandaga, Agustiadi, Teguh, Kuswardani, Anastasia, Mbay, Nurman, Setiawan, Agus, 2019. Makassar strait throughflow seasonal and interannual variability, an overview. J. Geophy. Res. Ocean: Recent Progress. Oceanograph Air-Sea Interact. Southeast Asian Archipelago 124, 3724–3736. https://doi.org/10.1029/2018JC014502.
Gruenburg, L.K., Gordon, A.L., 2018. Variability in makassar strait heat flux and its effect on the eastern tropical Indian Ocean. In: Durack, Paul J. (Ed.), Oceanography (Wash. D. C.) 31 (2), Guest. https://doi.org/10.5670/oceanog.2018.220. Lars H. Smedsrud Alex Sen Gupta.
Gruenburg, L.K., Gordon, A.L., Thurnherr, A.M., 2023. Indonesian throughflow partitioning between Leeuwin and south equatorial currents. J. Phys. Oceanogr. 53 (9), 2159–2170.
Hu, D., Wang, F., Sprintall, J., Wu, L., Riser, S., Cravatte, S., Gordon, A., Zhang, L., Chen, D., Zhou, H., Ando, K., 2020. Review on observational studies of western tropical Pacific Ocean circulation and climate. J. Oceanol. Limnol. 38 (4), 906–929.
Kersalé, M., Volkov, D.L., Pujiana, K., Zhang, H., 2022. Interannual variability of sea level in the southern Indian Ocean: local vs. remote forcing mechanisms. Ocean Sci. 18 (1), 193–212.
Kundu, P.K., McCreary Jr, J.P., 1986. On the dynamics of the throughflow from the Pacific into the Indian Ocean. J. Phys. Oceanogr. 16 (12), 2191–2198.
Li, J., Li, Y., Guo, Y., Li, G., Wang, F., 2023. Decadal variability of sea surface salinity in the Southeastern Indian Ocean: roles of local rainfall and the Indonesian throughflow. Front. Mar. Sci. 9, 1097634.
Menezes, V.V., Phillips, H.E., Vianna, M.L., Bindoff, N.L., 2016. Interannual variability of the south Indian countercurrent. J. Geophys. Res.: Oceans 121 (5), 3465–3487.
Roach, A.T., Aagaard, K., Pease, C.H., Salo, S.A., Weingartner, T., Pavlov, V., Kulakov, M., 1995. Direct measurements of transport and water properties through the bering strait. J. Geophys. Res. 100, 18443–18458.

Ridgway, K.R., Condie, S.A., 2004. The 5500-km-long boundary flow off western and southern Australia. J. Geophys. Res.: Oceans 109 (C4).
Schmitz, Jr.W.J., 1995. On the interbasin-scale thermohaline circulation. Rev. Geophys. 33 (2), 151–173.
Smith, R.L., Huyer, A., Godfrey, J.S., Church, J.A., 1991. The Leeuwin current off western Australia, 1986–1987. J. Phys. Oceanogr. 21 (2), 323–345.
Song, Q., Gordon, A.L., Visbeck, M., 2004. Spreading of the Indonesian throughflow in the Indian Ocean. J. Phys. Oceanogr. 34, 772–792. https://doi.org/10.1175/1520-0485(2004)034<0772:SOTITI>2.0.CO, 2.
Speich, S., Blanke, B., de Vries, P., Döös, K., Drijfhout, S., Ganachaud, A., Marsh, R., 2002. Tasman leakage: a new route for the global conveyer belt. Geophys. Res. Lett. 29, 10–13.
Speich, S., Blanke, B., Cai, W., 2007. Atlantic meridional overturning circulation and the Southern Hemisphere supergyre. Geophys. Res. Lett. 34, 1–5. https://doi.org/10.1029/2007GL031583.
Sprintall, J., Biastoch, A., Gruenburg, L.K., Phillips, H.E., 2024. Oceanic basin connections. In: The Indian Ocean and Its Role in the Global Climate System. Elsevier, pp. 205–227.
Taburet, G., Sanchez-Roman, A., Ballarotta, M., Pujol, M.-I., Legeais, J.-F., Fournier, F., et al., 2019. Duacs DT2018: 25 years of reprocessed sea level altimetry products. Ocean Sci. 15 (5), 1207–1224. https://doi.org/10.5194/os-15-1207-2019.
Talley, L.D., 2013. Closure of the global overturning circulation through the Indian, Pacific, and Southern Oceans: schematics and transports. Oceanography (Wash. D. C.) 26 (1), 80–97. https://doi.org/10.5670/oceanog.2013.07.
Terrell, G.R., Scott, D.W., 1992. Variable kernel density estimation. Ann. Stat. 1236–1265.
Toole, J.M., Warren, B.A., 1993. A hydrographic section across the subtropical South Indian Ocean. Deep Sea Res. Oceanogr. Res. Pap. 40 (10), 1973–2019.
van Sebille, E., Sprintall, J., Schwarzkopf, F.U., Gupta, A.S., Santoso, A., England, M.H., Biastoch, A., Boning, C.W., 2014. Pacific-to-Indian Ocean connectivity: tasman leakage, Indonesian throughflow, and the role of ENSO. J. Geophys. Res. Oceans 119. https://doi.org/10.1002/2013JC009525.
Vinogradova, N., Lee, T., Boutin, J., Drushka, K., Fournier, S., Sabia, R., Stammer, D., Bayler, E., Reul, N., Gordon, A., Melnichenko, O., 2019. Satellite salinity observing system: recent discoveries and the way forward. Front. Mar. Sci. 6, 243.
Waite, A.M., Thompson, P.A., Pesant, S., Feng, M., Beckley, L.E., Domingues, C.M., Gaughan, D., Hanson, C.E., Holl, C.M., Koslow, T., Meuleners, M., 2007. The Leeuwin Current and its eddies: an introductory overview. Deep Sea Res. Part II Top. Stud. Oceanogr. 54 (8–10), 789–796.
Zheng, S., Feng, M., Du, Y., Meng, X., Yu, W., 2018. Interannual variability of eddy kinetic energy in the subtropical southeast Indian Ocean associated with the El Niño-Southern Oscillation. J. Geophys. Res.: Oceans 123 (2), 1048–1061.